OPTIMIZATION AND TESTING OF FLAT-PLATE TRAILING-EDGE SERRATION GEOMETRY FOR REDUCING AIRFOIL SELF-NOISE

Basim Al Tlua*[1] and Joana Rocha†[1]
Department of Mechanical and Aerospace Engineering, Carleton University, Ottawa, Ontario

Résumé

Avec une utilisation du trafic aérien et un réseau de transport en expansion, le bruit émis par les avions civils durant le décollage et l'atterrissage est devenu une préoccupation majeure pour les communautés vivant proches des aéroports. L'objectif de ce travail est d'étudier la réduction du bruit d'interaction Turbulente en Couche Limite-Bord de Fuite (TCL-BF). Afin de tester le concept de réduction du bruit, la configuration expérimentale requise est conçue et créée. La première partie de cette étude porte sur le développement d'une section d'essai en soufflerie aéroacoustique à l'Université Carleton. Les murs de la section d'essai ont été traités acoustiquement pour simuler un environnement acoustique en champ lointain avec une transmission en vol. Les deux côtés de la section d'essai en soufflerie sont équipés de chambres anéchoïques et revêtus d'écrans en tissu tendu à transparence acoustique qui agissent comme une interface entre la section d'essai et les chambres anéchoïques. Cela fourni une surface d'écoulement lisse tout en éliminant le besoin d'un receveur de jet et permet de réduire les effets d'interférence. La capacité à réduire le bruit TCL-BF par des dentelures de bord de fuite est d'abord analysée par une étude d'optimisation numérique, et les bords de fuite sont ensuite testés en soufflerie. Trois géométries de dentelure différentes sont étudiées. Les spectres de bruit ont été modélisés à l'aide du modèle semi-empirique de Howe pour une plaque plate semi-infinie, à angles d'attaque nuls et à faible nombre de Mach. Le profil aérodynamique NACA 0012 et les bords de fuite plats sont analysés et testés. Les résultats des études d'optimisation sont utilisés pour examiner l'influence des paramètres de conception de dentelure. On montre que les bords de fuite dentelés en dents de scie produisent des réductions de bruit plus importantes que les bords de fuite fendus et sinusoïdaux. Les résultats expérimentaux et d'optimisation sont ensuite comparés. Il est conclu que les résultats numériques et expérimentaux sont en accord montrant que les configurations de bord de fuite dentelées optimisées peuvent produire moins de bruit TCL-BF par rapport à la configuration de bord de fuite droit traditionnel.

Mots clefs : Bruit d'aéronef, conception de vent d'aéronef, couche limite turbulente, bruit de bord de fuite

Abstract

With an expanding network of transportation and the use of air traffic, noise radiated from civil aircraft during takeoff and landing have become a major concern to communities nearby airports. The objective of this work is to investigate the reduction of Turbulent Boundary Layer-Trailing Edge (TBL-TE) interaction noise. In order to test the concept of noise reduction, the required experimental setup is designed and created. The first part of this study focuses on developing an aeroacoustic wind tunnel test section at Carleton University. The test section walls have been acoustically treated to simulate an acoustically far-field environment with forwarding flight. The two sides of the wind tunnel test section are fitted with anechoic chambers and lined with acoustic transparency tensioned cloth screens which act as an interface between the test section and the anechoic chambers to provide a smooth flow surface while eliminating the need for a jet catcher and reducing interference effects. The ability of the trailing edge serrations to reduce TBL-TE noise is first analyzed through numerical optimization study, and trailing edges are after tested in a wind tunnel. Three different serration geometries are investigated. The noise spectra were modelled using Howe semi-empirical model for a semi-infinite flat plate, at zero angles of attack and low Mach number. NACA 0012 airfoil and flat-plate trailing edges are analyzed and tested. The results of the optimization studies are used to examine the influence of serration design parameters. It is shown that the sawtooth serrated trailing edges yield greater noise reductions than slitted and sinusoidal serrated trailing edges. Experimental and optimization results are then compared. It is concluded that numerical and experimental results are in agreement showing that optimized serrated trailing edge configurations can yield less TBL-TE noise compared to the traditional straight-trailing edge configuration.

Keywords: Aircraft noise, aircraft wind design, turbulent-boundary layer, trailing edge noise.

1 Introduction

The noise produced at and near airports is a major source of noise to surrounding communities, airport employees and, people that travel frequently. Aircraft noise has always been undesirable, and in recent years several studies have been released that make a significant connection between exposure to aircraft noise and an increased risk of cardiovascular diseases [1-3]. The problem of aircraft noise then becomes much larger when considering trends in the aerospace industry that

include increasing aircraft size and speed as well as major increases in the volume of air traffic [4]. The two segments of an aircraft's flight where the most amount of noise is radiated to nearby communities are the take-off and landing phases. During the landing phase, while the engine throttle is turned down significantly, an important source of noise arises from the turbulent boundary layers (TBL) flow-structures convecting downstream across solid surfaces and interacting with the trailing edges. This mechanism of noise generation is known as the turbulent boundary layer-trailing edge (TBL-TE) noise, and its frequency spectrum is broadband in nature. TBL-TE noise is also a major source of noise in other applications, such as from wind turbines where exposure to nearby communities has been a complaint. With the growing global adaptation of alternative, environmentally friendly sources of energy, the implementation of wind turbine farms is quickly increasing. Consequently, the noise produced by wind turbines has become a significant issue in rural communities across the world where the wind farms are most often located [5].

Airframe noise research suggests that further research should be focused on noise generation mechanisms and noise reduction techniques. One promising method of reducing TBL-TE noise is by the addition of a flat-plate, serrated trailing edge extensions. This method of noise reduction has long been considered viable but has received increased attention in the last decade. The research has included experimental, theoretical and numerical studies [6-9] that have all shown the ability of trailing edge serrations to reduce TBL-TE noise. The amount of noise reduction and frequency ranges in which noise attenuation occurs varies between studies; however, it is generally agreed that for at least some part of the frequency spectrum, trailing edge serrations can produce TBL-TE noise reductions of a significant level [10].

Optimization studies have previously been conducted to reduce TBL-TE noise [11, 12]; however, they have mainly focused on altering the airfoil profile at and near the trailing edge. These studies were able to show that new, lower-noise designs could be generated through numerical optimization processes by using a semi-empirical model of noise prediction. General trends have been inferred from research involving the prediction of TBL-TE noise from serrated trailing edges.

The flow phenomena around aircraft components are complex [13-15], thus the noise generation mechanisms are difficult to be understood. Although the CFD combined with the acoustic analogy method has been widely applied in airframe noise prediction [16, 17], this method is costly and still lack of enough accuracy due to the limit of grid size, especially at high-frequency range. However, wind tunnel experiments can lead us to a better understanding of the noise mechanisms, and the results can also be used as benchmarks for the validation of numerical methods. Aeroacoustic experiments cannot be conducted at general wind tunnels due to the high background noise in the test section. A good acoustic facility must ensure a low background noise level to meet the essential requirement for aeroacoustic measurements, i.e., the background noise should be at least 10 dB lower than the noise radiated from models over a wide frequency range. The objective of this work is thus to study the predicted relative performance possibilities of trailing edge serration designs through numerical optimization, and design, manufacture, and test the optimized serration TE to confirm optimization results.

2 Wind tunnel characterization

The experiments were conducted in the medium-speed, subsonic, closed-loop wind tunnel at Carleton University (as shown in Figure. 1). The airflow is powered by a 37.3 kW (50 HP) variable-speed DC motor driving a 1.2 m axial propeller at speeds as high as 900 RPM. A variable frequency drive (VFD) modulates the rotational frequency of the fan at a resolution of 1.0Hz, and a pitot-static probe, located just downstream of the inlet, was used to calibrate the linear relationship between motor frequency and wind tunnel velocity. From the calibration, it was determined that the VFD could control the flow speed in increments of 0.9 m/s, up to a maximum speed of approximately 40 m/s. Nowadays, due to safety and component long-range issues, this velocity is limited, in this study, to 35 m/s. A series of turbulence grids precede a 9:1 contraction, which reduces the turbulence intensity levels in the center of the test section to less than 0.27%, as measured for speeds up to 15 m/s. The tunnel has a removable, rectangular test section measuring 1.83 m in length and 0.78 m x 0.51 m at the inlet in width and height, respectively.

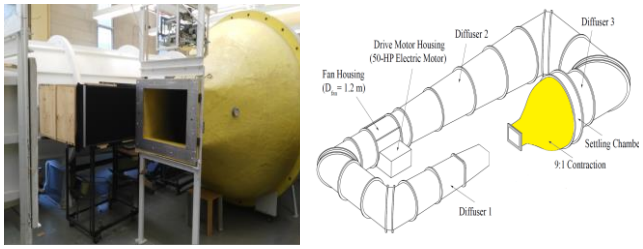

Figure 1 : Wind tunnel at Carleton University

3 New aeroacoustic test section

A new test section (shown in Figures 2 and 3) along with the surrounding anechoic chambers was completed to be used for aeroacoustic testing. This test section is a 0.78 m x 0.51 m rectangular section, 1.83 m long. The upper and lower walls of the test section are each composed of two aluminum sheet panels and contain hardware (circle aluminum material) for the vertical mounting of a two-dimensional airfoil (shown in Figure 3) midway between the acoustic windows (i.e. test section side walls), and 0.45 m from the upstream end of the test section. The two sides of the walls of the test section are made of stretched, thin-weave cloth covering a streamwise length of 1.83 m, which provides a smooth flow surface, similar to that of a hard-walled test section, and also a significant reduction in the lift interference effects when compared to that of an open-jet test section. The cloth window allows sound to pass through the walls into the anechoic chambers with very little attenuation.

* basim.altlua@carleton.ca
† Joana.Rocha@carleton.ca
‡

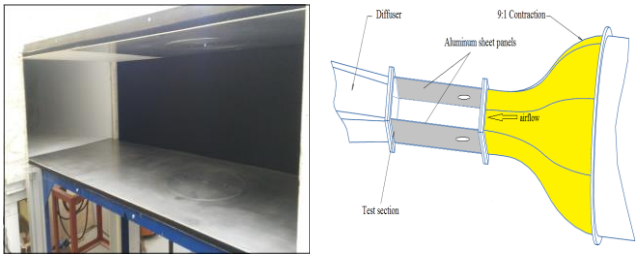

Figure 2 : Aeroacoustic test section

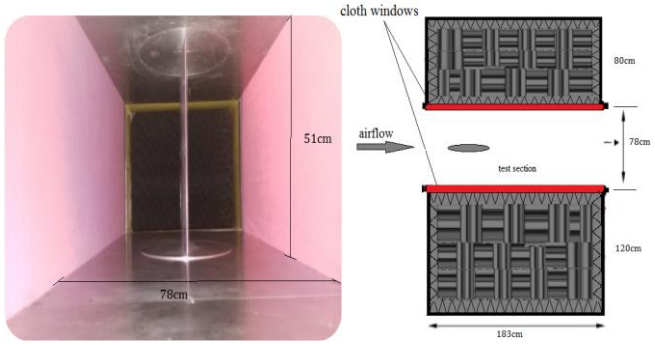

Figure 3 : Right: a cross-section through the aeroacoustics test section and anechoic as seen from above. Left: photograph was taken from downstream showing the test section interior

4 Anechoic system

4.1 Design considerations

The design of an anechoic system in the wind tunnel aims to achieve low noise radiation and low residual turbulence in the freestream. Besides acoustic and aerodynamic requirements to design anechoic system, there are also budgetary limits, as well as limits for available facility space that must be considered. The acoustical performance target is decided upon by the background noise to be at least 10 dB lower than the airfoil/flat-plate trailing edge self noise at a freestream velocity. The overall layout of the close wind tunnel with respect to the anechoic chamber, as well as some of the design details for each wind tunnel components, will be presented in the next sections.

4.2 Physical layout

The wind tunnel has an anechoic system that consists, primarily, of an aeroacoustic test section and two anechoic chambers (shown in Figure 3). The two anechoic chambers are positioned on either side of the aeroacoustic test section to capture the sound emitted through the acoustic windows and reduce sound reflections inside the section. The chambers are joined together with bolts and clamps to maintain a pressure seal. Both chambers have the same streamwise length of 1.83 m and different depths of 0.8 m right-side, and 1.2 m left-side. The chambers are lined with 0.015 m carpet bed and, 0.05 m acoustic wedged foam designed to reduce acoustic reflections.

Each chamber is sealed to the test section so that there is no airflow through either acoustic window. The regions around each of the acoustic windows are covered with a carpet-bed and acoustic foam transitions to cover up all of the hard surfaces within the chamber. The chambers are equipped with a door for access to the inside of the chamber, and for installation of data acquisition equipment. The entire system is removable so that the wind tunnel can be switched from a hard-walled configuration to an anechoic, and back again.

4.3 Acoustic transparency of the cloth windows

As with the characterization of the anechoic chambers, the acoustic transparency of the cloth windows used for the current study is discussed in detail in Remillieux et al. [18]. To investigate the acoustic transparency of the cloth sheet windows, the loudspeaker as a white noise source placed perpendicular to the window in the suction side of the anechoic chamber at a distance of 0.05 m from the window and a single calibrated microphone (Bruel & Kjaer (B&K) 4944-A, ¼ inch) was used on the other side of the window to record the sound pressure of the source as shown in Figure 4.

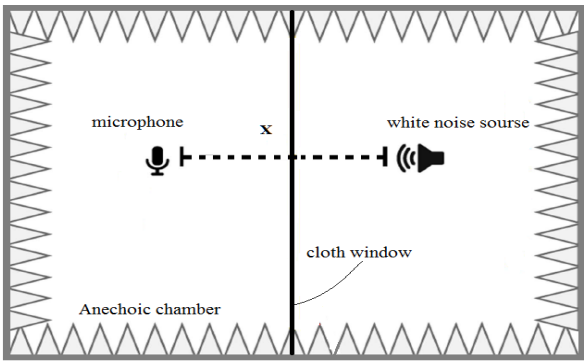

Figure 4 : Acoustic transparency of the cloth window

The sound levels, white noise, generated by the source were measured and were compared to the measured levels that the microphone would have been exposed to in the absence of the window. Sound pressure level (SPL) was used to compare the noise levels measured in the anechoic enclosure to those measured in the presence of the cloth window. The measurement is presented in Figure 5.

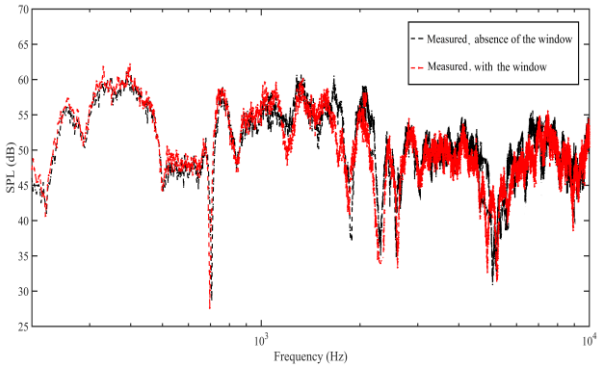

Figure 5: Attenuation of sound passing through the acoustic cloth window as a function of frequency.

Figure 5 shows that there is minimal loss through the window (~<3dB) for frequencies less than 10kHz. For all measurements presented in this paper, the frequency range of

interest is significantly less than 10 kHz and thus the acoustic loss through the sheet windows can be neglected.

5 Airfoil model

For some of the tests, a NACA 0012 airfoil model was used as a benchmark test. The chord of the airfoil is 0.3 m, and the span is 0.51m. The 2D airfoil is manufactured as two halves, each one composed of three pieces with eight screws (see Figure 6). Eight holes were drilled on each side of the chord length of the airfoil, so this can be fixed on the circle rotating mechanism. The trailing edge is 0.08 m wide. The NACA 0012 airfoil wing is mounted vertically in the test section with its leading-edge (at zero angles of attack) 0.45 m downstream of the test section entrance. Angles relative to zero were set by using a calliper and scribe lines on the steel floor plate immediately beneath the model.

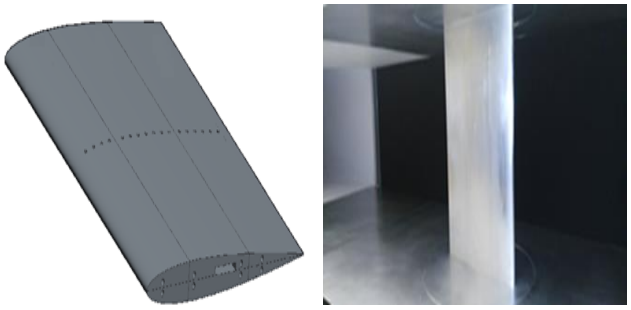

Figure 6: 2-D airfoil schematic.

6 Noise source model

In this section, the mathematical models for the prediction of noise used in this paper are presented. The underlying derivation for the noise models was originally given by Howe for sinusoidal serrations [6], and then soon after for sawtooth serrations [7]. In recent years, the model for slitted trailing edge serrations was presented by Gruber et al [19]. The modelling is based on Howe's derivation of the problem [7] which pressure fluctuations in the TBL are scattered into radiated noise by the discontinuity in the acoustic impedance that occurs at the trailing edge and includes the following assumptions:

- The flow is of low Mach number.
- The model has infinite span.
- Frozen turbulence convected past the trailing edge of a semi-infinite flat plate.
- The Kutta condition is satisfied.
- No other extraneous noise sources are present.

Figure 7 shows a sketch of the the four geometries considered in this study. The expressions defining the sawtooth, slitted and sinusoidal geometry are given in Eqs. 1, 2 and 3, respectively.

Sawtooth edge :

$$y_1 = \Gamma(y_3) = \begin{cases} (4h/\lambda)(y_3 - n\lambda), & n\lambda < y_3 < (n+0.5)\lambda \\ -(4h/\lambda)(y_3 - n\lambda), & (n-0.5)\lambda < y_3 < n\lambda' \end{cases} \quad (1)$$

$$\mathrm{n} = 0, \pm 1, \pm 2, \pm 3, \ldots$$

Slitted edge

$$y_1 = \Gamma(y_3) = \begin{cases} -h, & n(\lambda_1 + \lambda_2) < y_3 < (n+1)\lambda_1 + n\lambda_2 \\ h, & (n+1)\lambda_1 + n\lambda_2 < y_3 < (n+1)(\lambda_1 + \lambda_2)' \end{cases} \quad (2)$$

$$\mathrm{n} = 0, \pm 1, \pm 2, \pm 3, \ldots$$

Sinusoidal edge:

$$y_1 = \Gamma(y_3) = h\cos\left(\frac{2\pi y_3}{\lambda}\right) \quad (3)$$

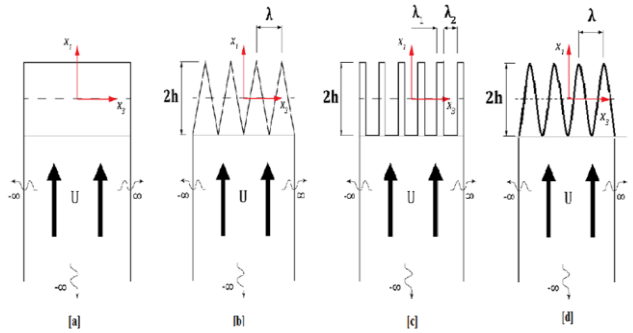

Figure 7: 2-D schematic drawings of flat plate [a] Straight, [b] Swa-tooth [c] Slitted and, [d] Sinusoidal TE extensions.

The scattered pressure produced at the trailing edge is defined in terms of the Green's function and the turbulence blocked pressure, P_b, as follows [7]:

$$P_s(\mathbf{x},\omega) = \frac{i}{2}\int_{-\infty}^{\infty} \mathrm{d}y_3 \int_{-\infty}^{\Gamma(y_3)} \mathrm{d}y_1 \times \int_{-\infty}^{\infty} \gamma(K)[\mathrm{G}(\mathbf{x}, y_1, y_3; \omega)]\, \mathrm{P_b}(\mathbf{K}; \omega) \mathrm{e}^{\mathrm{i}(K_1 y_1 + K_3 y_3)} \mathrm{d}^2\mathbf{K} \quad (4)$$

where $\mathbf{K} = (K_1, 0, K_3)$ is the boundary layer turbulent wave-number vector, and $\gamma(K) = \sqrt{(\kappa^2 - |\mathbf{K}|^2)}$, for $\kappa > |\mathbf{K}|$ and $\gamma(K) = i\sqrt{(|\mathbf{K}|^2 - \kappa^2)}$, for $\kappa < |\mathbf{K}|$.

The Green's function is given by Howe in [6] and is based on applying the slender-wing approximation to the Green's function for straight trailing edges. P_b is obtained from an empirical model for the turbulent wall pressure wave-number-frequency spectrum developed by Chase [20]:

$$P_s(\mathbf{x},\omega) = \frac{C_m \rho^2 u_*^3 K_1^2 \delta^5}{\left[\left(K_1 - \frac{\omega}{U_c}\right)^2 \left(\frac{\delta U_c}{3u_*}\right) + (\mathbf{K}\delta)^2 + \varepsilon^2\right]^{\frac{5}{2}}} \quad (5)$$

in which the friction velocity, $u_* = 0.03U$, the convection velocity, $U_c = 0.7U$, and the empirical constants, $C_m = 0.1553$ and $\varepsilon = 1.33$.

The final, non-dimensional, forms of the trailing edge noise spectrum for the straight, sawtooth, slitted and sinusoidal trailing edge geometries are the following:

$$\Psi_0(\omega) = \frac{\left(\frac{\omega\delta}{U_c}\right)^2}{\left[\frac{\omega\delta}{U_c} + \varepsilon^2\right]^2} \quad (6)$$

$$\Psi_{Saw}(\omega) = 8\left(\frac{h}{\delta}\right)^2\left(\frac{\omega h}{U_c}\right)\times \sum_{n=-\infty}^{\infty}\frac{\left[1-\cos\left(\frac{2\omega h}{U_c}\right)/\cos(n\pi)\right]\left[\left(\frac{\omega h}{U_c}\right)^2+\left(2n\pi\frac{h}{\lambda}\right)^2\right]}{\left[(n\pi)^2-\left(\frac{2\omega h}{U_c}\right)^2\right]^2\left[\left(\frac{\omega h}{U_c}\right)^2+\left(2n\pi\frac{h}{\lambda}\right)^2+\left(\frac{\varepsilon h}{\delta}\right)^2\right]^2} \quad (7)$$

$$\Psi_{Slit}(\omega) = \sum_{n=-\infty}^{\infty}\Theta\Theta^*\frac{\left[\left(\frac{\omega\delta}{U_c}\right)^2+\left(2n\pi\frac{\delta}{\lambda_1+\lambda_2}\right)^2\right]}{\left[\left(\frac{\omega\delta}{U_c}\right)^2+\left(2n\pi\frac{\delta}{\lambda_1+\lambda_2}\right)^2+(\varepsilon)^2\right]^2} \quad (8)$$

$$\Theta(K,\lambda_1,\lambda_2,h) = n^{-1}\left[\left(e^{\frac{2in\pi\lambda_1}{\lambda_1+\lambda_2}}-1\right)e^{iK_1h} + \left(1-e^{\frac{-2in\pi\lambda_1}{\lambda_1+\lambda_2}}\right)e^{-iK_1h}\right] \quad (9)$$

$$\Psi_{Sin}(\omega) = \left(\frac{\omega h}{U_c}\right)\sum_{n=-\infty}^{\infty}J_n^2\left(\frac{\omega h}{U_c}\right)\frac{\left|\left(\frac{\omega\delta}{U_c}\right)^2+\left(2n\pi\frac{\delta}{\lambda}\right)^2\right|}{\left[\left(\frac{\omega\delta}{U_c}\right)^2+\left(2n\pi\frac{\delta}{\lambda}\right)^2+\varepsilon^2\right]^2} \quad (10)$$

The boundary layer thickness, δ, at the airfoil trailing is an important parameter in determining the noise performance of trailing edge serrations. The TBL thickness used in the noise prediction is calculated as following [21, 22]:

$$\delta = \frac{0.37c\left[1+\left(\frac{R_{ec}}{6.9\times10^7}\right)^2\right]^{\frac{1}{10}}}{R_{ec}^{\frac{1}{5}}} \quad (11)$$

The non-dimensional overall sound pressure level ($OASPL_{norm}$) describes the total amount of noise produced across the desired frequency range. The $OASPL_{norm}$ is used both an objective function and for the comparison of various trailing edge designs to a straight trailing edge. The $OASPL_{norm}$ is calculated as follows:

$$OASPL_{norm} = 10\log_{10}\left(\int_{\omega_{min}}^{\omega_{max}}\Psi(\omega)d\omega\right) \quad (12)$$

where ω_{min} and ω_{max} are the lower and upper bounds on the frequency range of interest respectively and, $\Psi(\omega)$ can be obtained from any of Eqs. 6 to 10 according to the geometry of interest.

7 Numerical optimization methods

This study examines three different optimization problems, which are given below in proper form in Eqs. (13) to (15). These equations correspond to the single-size optimization of sawtooth (see Figure 6b), slitted (see Figure 6c) and sinusoidal (see Figure 6d) TE geometries, respectively. In each case, the optimum design is the single-size of serration that produces the least amount of total noise overall frequencies between 0.1 Hz and 10 kHz.

$$\begin{aligned}&\underset{h,\lambda}{\text{minimize}} && Z = OASPL_{norm\_saw}(h,\lambda),\\ &\text{subject to} && 0 \le h \le h_{max}\\ & && \lambda_{min} \le \lambda \le \lambda_{max}\end{aligned} \quad (13)$$

$$\begin{aligned}&\underset{h,\lambda}{\text{minimize}} && Z = OASPL_{norm\_slit}(h,\lambda_1,\lambda_2),\\ &\text{subject to} && 0 \le h \le h_{max}\\ & && (\lambda_1)_{min} \le \lambda_1 \le (\lambda_1)_{max}\\ & && (\lambda_2)_{min} \le \lambda_2 \le (\lambda_2)_{max}\end{aligned} \quad (14)$$

$$\begin{aligned}&\underset{h,\lambda}{\text{minimize}} && Z = OASPL_{norm\_sinu}(h,\lambda),\\ &\text{subject to} && 0 \le h \le h_{max}\\ & && \lambda_{min} \le \lambda \le \lambda_{max}\end{aligned} \quad (15)$$

where Z is the objective function value; h_{max} is the largest feasible serration amplitude corresponding to the sawtooth, slitted and sinusoidal geometries accordingly; (λ_{min}) and (λ_{max}) are the smallest and largest feasible sawtooth and sinusoidal widths, respectively; $(\lambda_1)_{min}$ and $(\lambda_1)_{max}$ are the smallest and largest feasible slit widths, respectively; and $(\lambda_2)_{min}$ and $(\lambda_2)_{max}$ are the smallest and largest feasible gap widths, respectively. A summary of the optimization studies conducted for this work is presented in Table 1.

8 Results and discussion

8.1 Background noise levels

The background noise of the wind tunnel is measured in the anechoic chamber with a single calibrated B&K microphone. Figure 8 shows empty test-section background sound pressure levels (SPL) in the starboard-side anechoic chamber as a function of flow speed, 0 m/s to 24 m/s. These measurements were made 1.4 m from the test-section center.

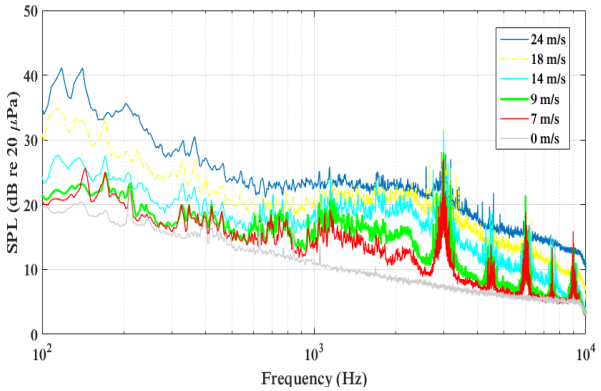

Figure 8: SPL in the starboard-side anechoic chamber (1.4 m from the test-section center) as a function of flow speed in the empty test section.

The highest spectral level can be seen at low frequencies (100-500 Hz). Background noise levels at frequencies less than 500 Hz are mostly tones generated by the wind tunnel

Table1: Optimization trials and associated design variable bounds for U = 24m/s.

Study No	Geometry	Lower Design Variables Bound (mm)			Upper Design Variables Bound (mm)		
		λ_{1min}	λ_{2min}	h_{min}	λ_{1max}	λ_{2max}	h_{max}
SS-Saw-1	Sawtooth	10	-	0	30	-	35
SS-Saw-2	Sawtooth	15	-	0	35	-	40
SS-Saw-3	Sawtooth	20	-	0	40	-	30
SS-Saw-4	Sawtooth	25	-	0	35	-	37.5
SS-Slit-1	Slitted	10	10	0	40	30	35
SS-Slit-2	Slitted	15	20	0	35	40	40
SS-Slit-3	Slitted	10	25	0	30	35	37.5
SS-Slit-4	Slitted	20	20	0	30	40	40
SS-Sinu-1	Sinusoidal	15	-	0	40	-	35
SS -Sinu-2	Sinusoidal	10	-	0	35	-	30
SS -Sinu-3	Sinusoidal	20	-	0	45	-	40
SS -Sinu-4	Sinusoidal	25	-	2	30	-	37.5

fan and levels at frequencies greater than 500 Hz are primarily broadband and believed to be due to a combination of oise sources including the fan, turning vanes, and scrubbing noise from flow surfaces in and around the test section. The peaks showed in 3 kHz, 4.5 kHz and 6 kHz are mostly associated with motor tones.

The Overall Sound Pressure Level, OASPL, is obtained by integrating the noise spectrum from 0.1 kHz to 10 kHz. Figure 9 shows the dependence of OASPL on free-stream velocity; the 5th power law is satisfied, which is similar to other closed-circuit type wind tunnels.

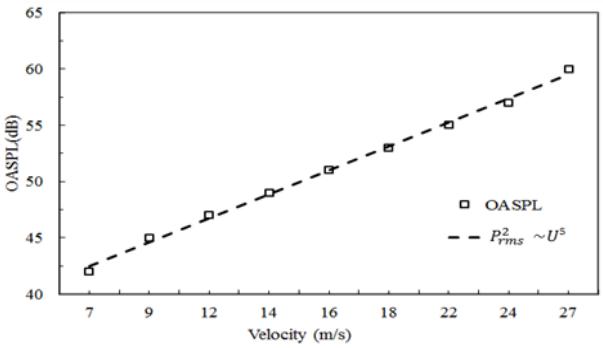

Figure 9 : The overall sound pressure level of background noise as a function of free-stream velocity.

To estimate the acoustic performance, the A-weighted overall sound pressure level, OASPL, is compared to other acoustic facilities around the world. Since the nozzle dimensions and microphone positions are different from each other, the measured results must be transformed before comparing with each other [7]:

$$\mathrm{OASPL}_{\mathrm{corrected}} = \mathrm{OASPL}_{\mathrm{measured}} - 10\log_{10}(S/R^2) \qquad (16)$$

where R and S are the distance from the microphone to the wind tunnel center-line and nozzle exit area, respectively.

The background noise of Carleton University wind tunnel is scaled using Eq. 16, and the results are shown in Figure 10. The background noise of other acoustic facilities with data obtained from the literature [23-26] is also plotted in Figure 10 for comparison. The results indicate that the background noise of the Carleton University wind tunnel is comparable with other aeroacoustic wind tunnels.

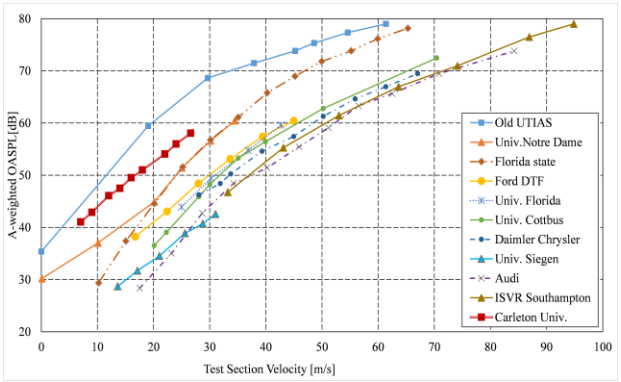

Figure 10: Comparison of A-weight sound pressure level of Carleton University wind tunnel to other acoustic facilities worldwide.

8.2 Far-field trailing edge noise measurements

Measurements of the airfoil TE noise

NACA0012 airfoil with straight and sawtooth trailing edge (see Figure 11) was submerged within the potential core of the jet to assess the trailing edge self-noise in relation to the wind tunnel background noise. The airfoil was held at zero angles of attack by side plates extended from the nozzle sidewalls. The radiated noise was measured at 1.4 m from the center of the trailing edge in the starboard-side, which corresponds to a 90^0 of polar angle θ.

At first, the background noise of the wind tunnel was measured under a freestream velocity of 14 m/s and 24 m/s. The airfoil with straight TE as a reference and the same airfoil with sawtooth TE were then attached to the sidewalls, and the same freestream velocities were repeated. The result of the TE self-noise spectra of these cases is plotted in Figure 11. The Figure shows that the serration geometry is effective in reducing the trailing edge noise component. The TE self-noise measurement is seen to be from ~5 to ~15 dB above the background wind tunnel noise within the frequency range from 0.1kHz to ~ 3kHz, which guarantees the validity of the results.

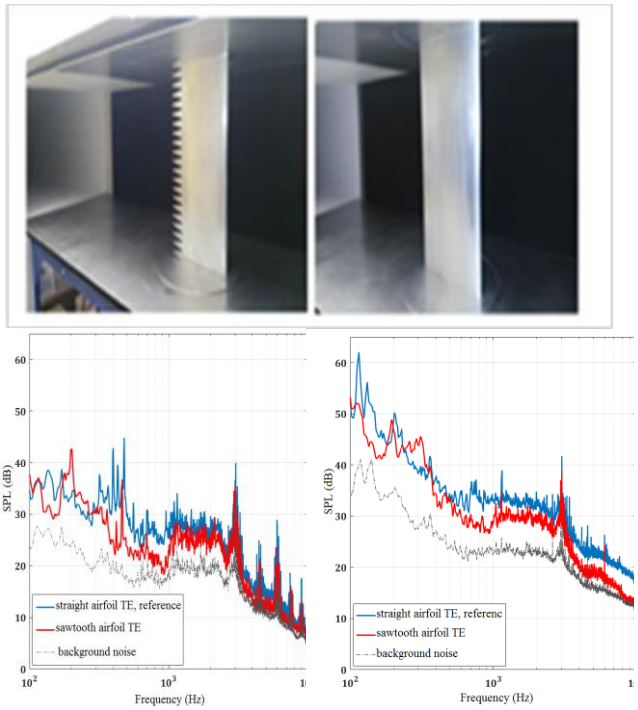

Figure 11: Measured SPL spectra for NACA0012 airfoil and the same airfoil with sawtooth TE at free-stream velocities of (Left) 14 m/s and (Right) 24 m/s at Carleton University anechoic wind tunnel. The background noise spectra are also shown in this figure for comparaison.

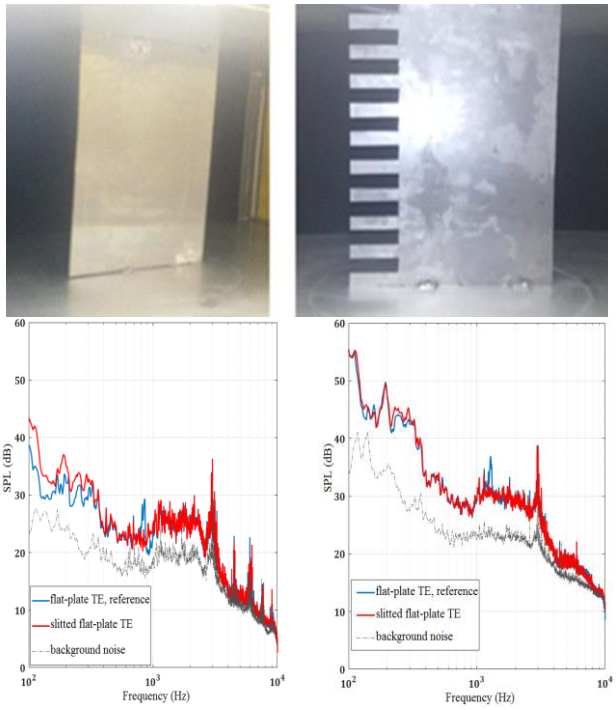

Figure 12 : Far-field acoustic spectra for the reference flat-plate and the flat-plate with trailing edge serrations, slitted TE, at freestream velocities of (Left) 14 m/s and (Right) 24 m/s. The background noise spectra are also shown in this figure for comparison.

Measurements of the flat-plate TE noise

A 3 mm thickness flat-plate, 0.30 m in a chord and 0.51 m in span, was submerged within the potential core of the jet to assess the trailing edge self-noise in relation to the wind tunnel background noise. The flat-plate was held at zero angles of attack by side plates extended from the nozzle sidewalls. The radiated noise was measured at 1.4 m from the center of the trailing edge in the starboard-side, which corresponds to a 90^0 of polar angle θ.

Similarly, to the airfoil, the background noise of the wind tunnel was measured first under a freestream velocity of 14 m/s and 24 m/s. The flat-plate with straight TE as a reference and the same flat-plate with slitted TE were then attached to the sidewalls, and the same freestream velocities were repeated. The result of the TE self-noise spectra of these cases is plotted in Figure 12. The figure indicates that the serration geometry is effective in reducing the trailing edge self-noise component and the TE self-noise measurement is seen to be from ~ 4 to ~16 dB above the background wind tunnel noise, within the frequency range from 0.1kHz to ~ 3kHz, which guarantees the validity of the results.

8.3 Optimization results

This section presents the optimization results from the analyses that used the sawtooth, slitted and sinusoidal geometry. The serrations' designs are optimized to find the single size of each tooth geometry that produces the least noise over the entire frequency spectrum of interest (0.1kHz to 10 kHz) for each set of constraints examined. A summary of the optimized designs from each study, and their respective $OASPL_{norm}$, is shown in Table 2.

Verification of the noise model

Noise models previously defined in Eqns. 6 to 10 were coded in Matlab to be used. In order to verify the Matlab code, the function outputs were compared to results published by Howe et al. [7] (for Eq. 7), by Azarpeyvand et al. [27] (for Eq. 8) and by Howe et al. [7] (for Eq. 10). Based on the thorough comparison in this analysis, it was concluded that the Matlab functions used produce identical results to the analytical equivalents, as shown in Figures 13, 14 and 15.

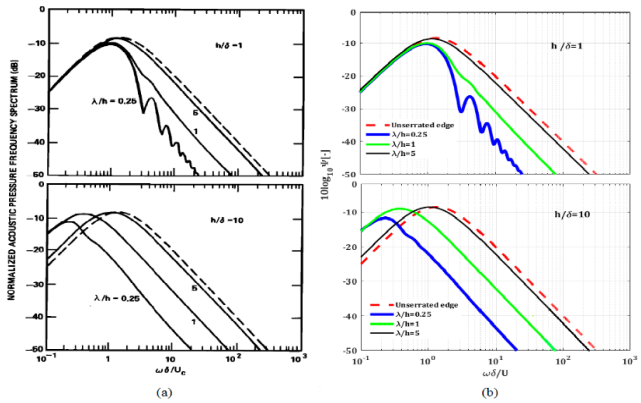

Figure 13: Normalized spectrum of noise produced by a low Mach number flow over a sawtooth TE: (a) from [7] Eqn. (17) ;(b) Matlab code.

Table2: Optimized designs from each study and noise produced by each trailing edge

Study No	Optimal Geometry (mm)			$OASPL_{norm}$ [dB]	$\int_{\omega_{min}}^{\omega_{max}} (\Psi i) = 10^{\frac{OASPL\_norm}{10}}$	$\Delta OASPL_{norm} = 10\log_{10}\left(\int_{\omega_{min}}^{\omega_{max}} \Psi_0 / \int_{\omega_{min}}^{\omega_{max}} \Psi_i\right)$
	λ_{1opt}	λ_{2opt}	h_{opt}			
Straight TE	-	-	-	30.1	1023.3	-
SS-Saw-1	10	-	35	16.7	46.7	13.3
SS-Saw-2	15	-	40	18.2	66.1	11.9
SS-Saw-3	20	-	30	21.5	141.2	8.6
SS-Saw-4	25	-	37.5	21.6	181.9	7.5
SS-Slit-1	10	10	6.4	27.9	616.6	2.2
SS-Slit-2	15	20	5.8	28.5	707.9	1.6
SS-Slit-3	10	25	6.0	28.5	707.9	1.6
SS-Slit-4	20	20	5.6	28.6	724.4	1.5
SS-Sinu-1	15	-	35	21.1	128.8	9
SS-Sinu-2	10	-	30	20.0	100	10.1
SS-Sinu-3	20	-	40	21.9	151.9	8.2
SS-Sinu-4	25	-	37.5	23.1	204.2	7

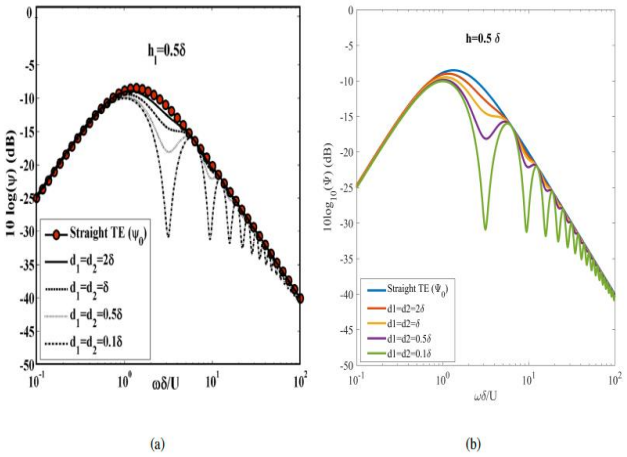

Figure 14: Normalized spectrum of noise produced by a low Mach number flow over a slitted TE: (a) from [27] Eqn. (10); (b) Matlab Code

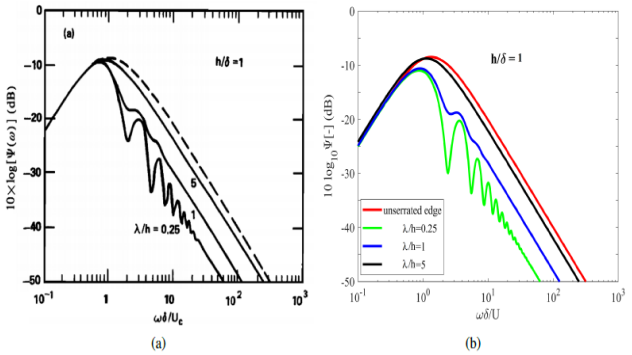

Figure 15. Normalized spectrum of noise produced by a low Mach number flow over a sinusoidal TE: (a) from [7] Eqn. (5.6); (b) Matlab Code.

Optimization of single-size sawtooth serrations

The noise spectrums for both a straight TE and each of the optimized, single-size, sawtooth TE designs are given in Figure 16. The optimized single-size sawtooth design, which produced the least noise, was obtained in the study of SS-Saw-1.

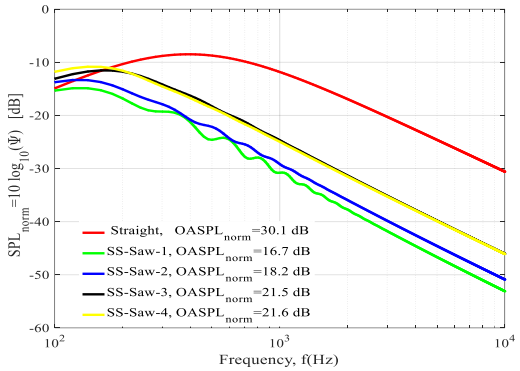

Figure 16. Normalized spectrum plotted as a function of frequency between 0.1kHz and 10kHz for $OASPL_{norm}$ optimized sawtooth trailing edge profiles.

This study applied the largest upper limit, and the smallest lower limit on h and λ respectively compared to the other studies in the SS-Saw group. The $OASPL_{norm}$ produced by SS-Saw-1 was 16.7 dB, corresponding to a 30.1 dB of a straight trailing edge and the reduction in $\Delta OASPL_{norm}$ is 13.1 dB compared to a straight trailing edge (see the Table 2 for more details).

Optimization of single-size slitted serrations

The noise spectrums for both a straight TE and each of the optimized, single-size, slitted TE designs are given in Figure 17. Of the single-size slit optimization studies, the design that produced the least noise was SS-Slit-1, which produced an $OASPL_{norm}$ of 27.9 dB corresponding to a 30.1 dB of a straight trailing edge and the reduction in $\Delta OASPL_{norm}$ is 2.2 dB compared to a straight trailing edge (see the Table 2 for more details). Similar to the single-size sawtooth optimization, SS-Slit-1 also applied the smallest lower limits on widths, λ_1 and λ_2 and the upper limit on the slit amplitude, h, is 6.4 dB. The optimum widths are seen to always be equal to their lower limits of $(\lambda_1)_{min}$ and $(\lambda_2)_{min}$.

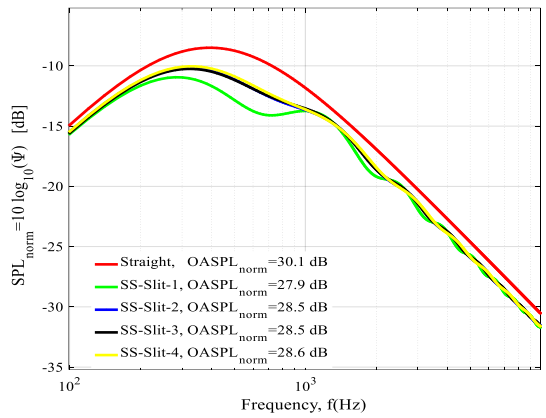

Figure 17: Normalized spectrum plotted as a function of frequency between 0.1KHz and 10kHz for OASPL$_{norm}$ optimized slitted trailing edge profiles

Optimization of single-size sinusoidal serrations

The noise spectrums for both a straight TE and each of the optimized, single-size, sinusoidal TE designs are given in Figure 18. The optimized single-size sinusoidal design, which produced the least noise, was obtained in the study of SS-Sinu-2.

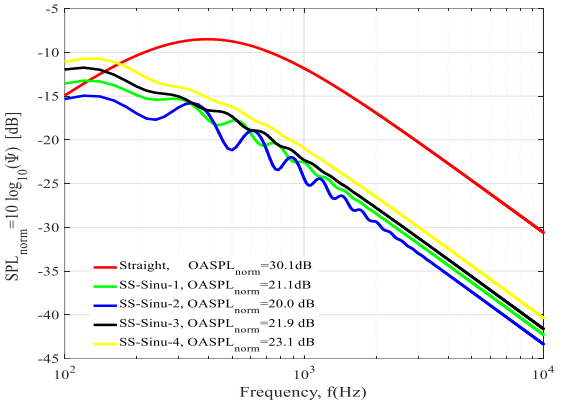

Figure 18. Normalized spectrum plotted as a function of frequency between 0.1kHz and 10kHz for OASPL$_{norm}$ optimized sinusoidal trailing edge profiles.

Similar to the single-size sawtooth optimization, this study applied the largest upper limit, and the smallest lower limit on h, and λ respectively compared to the other studies in the SS-Sinu group. The OASPL$_{norm}$ produced by SS-Sinu-2 was 20.0 dB, corresponding to a 30.1 dB of a straight trailing edge and the reduction in ΔOASPLnorm is 10.1 dB compared to a straight trailing edge (see the Table 2 for more details).

Each of the optimum designs in all studies, (see Figure 19), sawtooth, slitted and sinusoidal TE produces a lower OASPL$_{norm}$ than the straight TE ; however, significant variations are seen in the amount of reduction achieved between the three, TE designs. This observation suggests that the optimization process can produce TE serration designs that produce less noise than designs that have previously been studied, and whose dimensions were chosen manually. Furthermore, based on our analysis, the sawtooth serration, SS-Saw-1, provides the greatest noise reduction, ΔOASPL$_{norm}$, over a wide range of frequencies as shown in Figure 19.

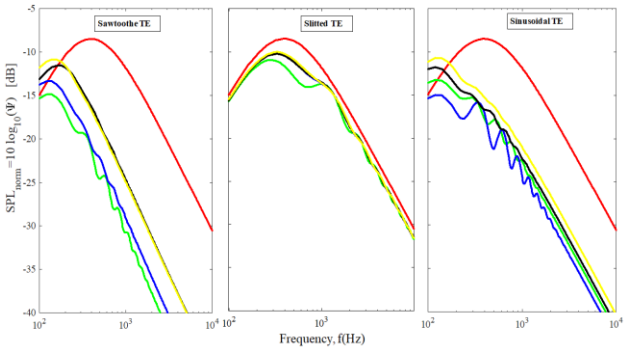

Figure 19: The compression between the optimum serrations.

8.4 Experimental results and comparison with numerical results

A comparison of the far-field noise SPL spectrum, measured at 90° overhead of the airfoil and flat-plate, trailing edge, between the best optimum serrated (SS-Saw-1, SS-Slit-1 and SS-Sinu-2) and the straight trailing edge, as defined in Table 2, is shown in Figure 20. Below ~250 Hz, an airfoil TE noise reduction relative to the straight trailing edge of between ~1 to ~ 6 dB can be seen for all trailing edge treatments.

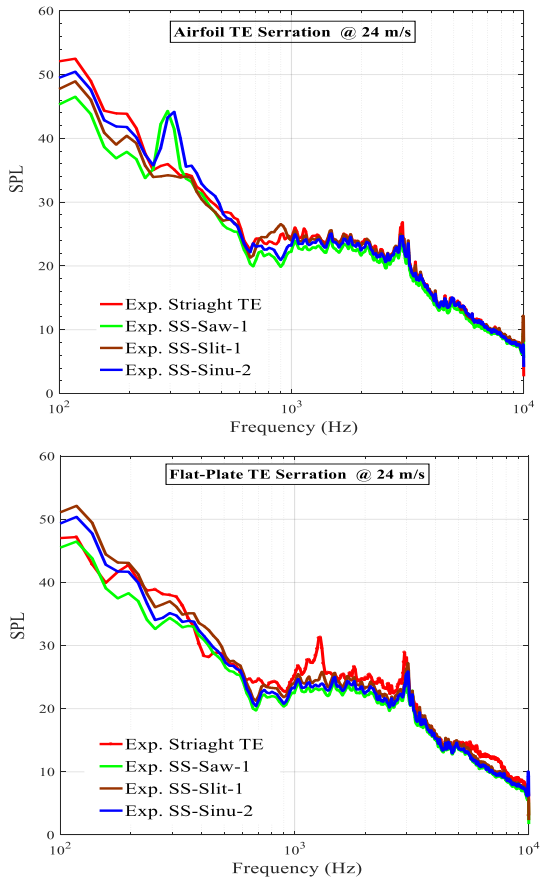

Figure 20: Measured far-field noise spectrum showing a comparison between straight and the sawtooth, slitted and sinusoidal TE with airfoil and flat-plate at 0^0 AoA and U= 24 m/s.

A comparison of the noise reduction, ΔSPL, between the predicted/optimized and experimental data for various optimum serrated trailing edges is shown in Figure 21. The level of predicted noise reduction is approximately ~29 to 52 dB higher than the measured reduction for SS-Saw-1 and SS-Sinu-2 and approximately ~1 to 3 dB for SS-Slit-1. This is in trend agreement with the previous results shown in [28] for sawtooth serrations. The predicted noise reduction tends to increase with frequency, while the measured one decreases with frequency.

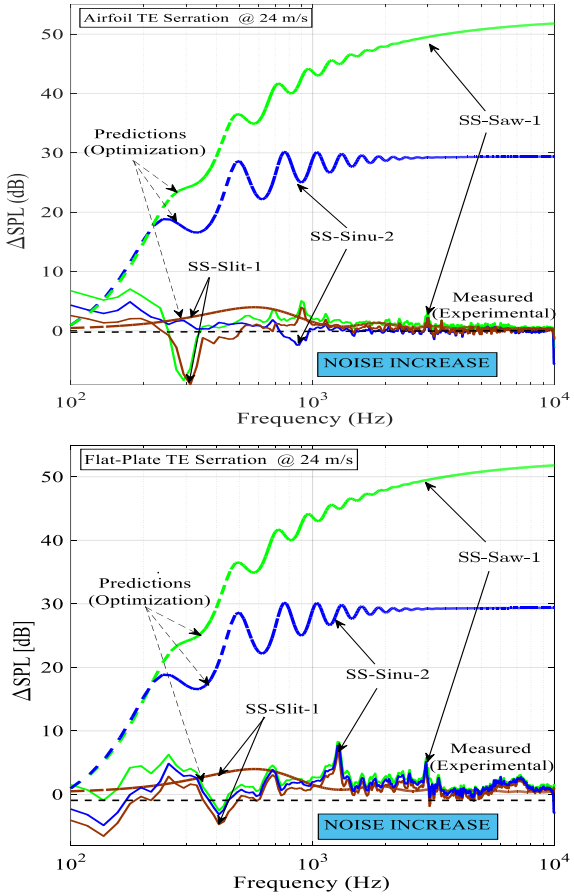

Figure 21 : Broadband noise reduction predicted by Howe (Dashed) and measured experimentally (Solid) for serration profiles SS-Saw-1, SS-Slit-1 and SS-Sinu-2 - Experimental data with airfoil and flat-plate at 0^0 AoA and U= 24 m/s.

The strong oscillations observed in the predicted noise reduction in Figure 21 are due to interference between the root and the tip of the serrations, which are not observed in the experimental data. Note that the oscillations observed in the experimental spectra are characteristics of trailing edge noise and are not related to the serrated edges as described by Amiet [29]. The predicted oscillations from the optimization are a direct consequence of Howe's model simplifying assumption; i.e., that the scattering process is the predominant source of TE noise with no extraneous sources present. However, experimental results suggest that extraneous noise sources may be present due to unsteadiness close to the serrations. While the noise reduction amounts from predictions and experimental data differ, Howe's model is still very useful for the optimization work to determine the best TE configurations which reduced the noise radiated

The discrepancies observed in Figure 21 between the optimization and measured noise reductions for serrated trailing edges speculates on the possible reasons:

- Assumption that the surface pressure in the boundary layer at the trailing edge is not affected by the serrations, but it is locally affected by the serration. However, this effect is likely to be small [28].
- The quadrupole sources in the boundary layer of the airfoil, upstream of the trailing are not accounted for in the theoretical far-field radiation.
- Numerically shown by Jones and Sandberg [30], the unsteadiness close to the serration due to horse-shoe vortices can be a source of extraneous noise

9 Conclusion

An aeroacoustic wind tunnel test section has been built at Carleton University. The tunnel has a rectangular test section with dimensions of 0.78 m in width, 0.51 m in height and 1.83 m long. Its aeroacoustic performance is measured. Results show that the background noise can be comparable with other aeroacoustic wind tunnels worldwide. A simplified airfoil and flat-plate TE noise are tested as a benchmark test. Results show that the serration geometry is effective in reducing noise and, the noise radiated from the TE is at least 10 dB higher than the background noise, satisfying the requirements for aeroacoustic measurements.

Three different geometrical profiles of trailing edge serrations have been optimized for the reduction of TBL-TE noise. The optimum width for the three, sawtooth, slitted and sinusoidal serrations, are the smallest allowable one in the overall spectrum frequencies. The optimum single-size sawtooth and sinusoidal always has the largest allowable amplitude whereas the optimum single-size slit has a specific amplitude value to optimize the balance.

Noise radiation from optimized trailing edges with different serrations, sawtooth, slitted and sinusoidal, has been investigated. It has been shown that the TE serration design can have a significant effect on the level of noise reduction. It has been shown that numerical and experimental results are in agreement showing that optimized serrated trailing edge configurations can yield less TBL-TE noise compared to the traditional straight trailing-edge configuration. Moreover, based on the optimization and experimental analyses, the sawtooth serration provides the greatest noise reduction over a wider range of frequencies when compared to slitted and sinusoidal TE serrations.

Acknowledgments

The first author likes to thank his supervisor, Prof. Joana Rocha, for all of her guidance and support.

References

[1] Correia AW, Peters JL, Levy JI, Melly S, Dominici F. Residential exposure to aircraft noise and hospital admissions for cardiovascular diseases: multi-airport retrospective study. Bmj. 2013 Oct 8;347: f5561.

[2] Kaltenbach M, Maschke C, Klinke R. Health consequences of aircraft noise. Deutsches Ärzteblatt International. 2008 Aug;105(31-32):548.

[3] Hansell AL, Blangiardo M, Fortunato L, Floud S, de Hoogh K, Fecht D, Ghosh RE, Laszlo HE, Pearson C, Beale L, Beevers S. Aircraft noise and cardiovascular disease near Heathrow airport in London: small area study. Bmj. 2013 Oct 8;347:f5432.

[4] Schaufele R. Federal Aviation Administration Aerospace Forecast: Fiscal Years 2016-2036, U.S. Department of Transportation, Rept. TC16-0002, Federal Aviation Administration, DC, Aug. 2016.

[5] Hansen K, Henrys N, Hansen C, Doolan C, Moreau D. Wind farm noise–what is a reasonable limit in rural areas?.

[6] Howe MS. Aerodynamic noise of a serrated trailing edge. Journal of Fluids and Structures. 1991 Jan 1;5(1):33-45.

[7] Howe MS. Noise produced by a sawtooth trailing edge. The Journal of the Acoustical Society of America. 1991Jul;90(1):482-7.

[8] Herr M. Design criteria for low-noise trailing-edges. In13th AIAA/CEAS Aeroacoustics Conference (28th AIAA Aeroacoustics Conference) 2007 May (p. 3470).

[9] Herr M. A noise reduction study on flow-permeable trailing-edges. CD Proceedings ODAS 2007. 2007.

[10] Chong TP, Vathylakis A. On the aeroacoustic and flow structures developed on a flat plate with a serrated sawtooth trailing edge. Journal of Sound and Vibration. 2015 Oct 13;354:65-90.

[11] Marsden AL, Wang M, Dennis JE, Moin P. Trailing-edge noise reduction using derivative-free optimization and large-eddy simulation. Journal of Fluid Mechanics. 2007 Feb;572:13-36.

[12] Bertagnolio F, Madsen HA, Bak C. Trailing edge noise model validation and application to airfoil optimization. Journal of Solar Energy Engineering. 2010 Aug 1;132(3).

[13] Xiao Z, Liu J, Luo K, Huang J, Fu S. Investigation of flows around a rudimentary landing gear with advanced detached-eddy-simulation approaches. AIAA journal. 2013 Jan;51(1):107-25.

[14] Pröbsting S, Serpieri J, Scarano F. Experimental investigation of aerofoil tonal noise generation. Journal of Fluid Mechanics. 2014 May;747:656-87.

[15] Lazos BS. Mean flow features around the inline wheels of four-wheel landing gear. AIAA journal. 2002 Feb;40(2):193-8.

[16] Kim T, Lee S. Aeroacoustic simulations of a blunt trailing-edge wind turbine airfoil. Journal of Mechanical Science and Technology. 2014 Apr 1;28(4):1241-9.

[17] Murayama M, Yokokawa Y, Yamamoto K, Hirai T. Computational study of low-noise fairings around tire-axle region of a two-wheel main landing gear. Computers & Fluids. 2013 Oct 1;85:114-24.

[18] Remillieux M, Crede E, Camargo H, Burdisso R, Devenport W, Rasnick M, Van Seeters P, Chou A. Calibration and demonstration of the new Virginia Tech anechoic wind tunnel. In14th AIAA/CEAS Aeroacoustics Conference (29th AIAA Aeroacoustics Conference) 2008 May (p. 2911).

[19] Gruber M, Azarpeyvand M, Joseph PF. Airfoil trailing edge noise reduction by the introduction of sawtooth and slitted trailing edge geometries. integration. 2010;10:6.

[20] Chase DM. The character of the turbulent wall pressure spectrum at subconvective wavenumbers and a suggested comprehensive model. Journal of Sound and Vibration. 1987 Jan 8;112(1):125-47.

[21] Wahidi R, Chakroun W, Al-Fahed S. The behavior of the skin-friction coefficient of a turbulent boundary layer flow over a flat plate with differently configured transverse square grooves. Experimental Thermal and Fluid Science. 2005 Nov1;30(2):141-52.

[22] Bies DA. A review of flight and wind tunnel measurements of boundary layer pressure fluctuations and induced structural response.

[23] Kim MS, Lee JH, Kee JD, Chang JH. Hyundai full scale aeroacoustic wind tunnel. SAE Technical Paper; 2001 Mar 5.

[24] Sarradj E, Fritzsche C, Geyer T, Giesler J. Acoustic and aerodynamic design and characterization of a small-scale aeroacoustic wind tunnel. Applied Acoustics. 2009 Aug 1;70(8):1073-80.

[25] MAEDA T, KONDO Y. RTRI's Large-scale low-noise wind tunnel and wind tunnel tests. Quarterly Report of RTRI. 2001;42(2):65-70.

[26] Chong TP, Joseph PF, Davies PO. Design and performance of an open jet wind tunnel for aero-acoustic measurement. Applied acoustics. 2009 Apr 1;70(4):605-14.

[27] Azarpeyvand M, Gruber M, Joseph P. An analytical investigation of trailing edge noise reduction using novel serrations. In19th AIAA/CEAS aeroacoustics conference 2013 (p. 2009).

[28] Gruber M, Joseph P, Chong TP. Experimental investigation of airfoil self noise and turbulent wake reduction by the use of trailing edge serrations. In16th AIAA/CEAS aeroacoustics conference 2010 (p. 3803).

[29] Amiet RK. Noise due to turbulent flow past a trailing edge. Journal of sound and vibration. 1976 Aug 8;47(3):387-93.

[30] Jones, L. E. and Sandberg, R. D., _Numerical investigation of airfoil self-noise reduction by addition of trailing-edge serrations, 16th AIAA/CEAS Aeroacoustics Conference, 2010.

Nomenclature

f	frequency
G(x,y;ω)	Green's function
h	serration amplitude
i	imaginary number
K	wavenumber vector
K_1	streamwise wavenumber
K_3	spanwise wavenumber
P_b	blocked pressure
P_s	scattered pressure
$\mathbf{R_{ec}}$	Reynolds number
U	mean flow speed
U_c	convection velocity (U_c=0.7U)
ω	angular frequency
χ_1, χ_2, χ_3	Cartesian coordinate system
Z	objective function value
$\Gamma(y_3)$	serration profile
λ	sawtooth and sinusoidal serration width
λ_1, λ_2	slitted serration width and gap width
δ	turbulent boundary layer thickness
κ	acoustic wavenumber (κ= ω/c)
ψ	non-dimensional trailing edge noise spectrum